JSS Focus Issue on Nanocarbons—In Memory of Sir Harry Kroto

Processing of Onion-like Carbon for Electrochemical Capacitors

Katherine L. Van Aken, Kathleen Maleski, Tyler S. Mathis, James P. Breslin, and Yury Gogotsi*,z

Department of Materials Science and Engineering and A.J. Drexel Nanomaterials Institute, Drexel University, Philadelphia, Pennsylvania 19104, USA

Multi-shell fullerenes known as onion-like carbon (OLC) are especially attractive in applications relative to energy storage, such as electrochemical capacitors, due to a near-spherical shape of particles, their nanoscale diameters and high conductivity leading to fast rate performance. Because of this, onion-like carbon can be fabricated into electrodes, used as a conductive additive, and may have potential in composites and additive manufacturing. However due to agglomeration of OLC particles, creating a stable, aqueous dispersion for ink production or formulating composites proves challenging. We explore how attrition milling, acid treatment, and probe sonication can be employed to decrease agglomeration and provide colloidal stability in aqueous media. We also investigate how the electrochemical performance changes with each processing step as well as the treatments in succession. When tested in electrochemical capacitors, the processing increases the capacitance by a factor of three, due to an added pseudocapacitive contribution which is not present in untreated OLC. As a result, the processing of OLC proves to be advantageous for the production of stable, aqueous solutions, which also exhibit improved electrochemical properties suitable for functional inks, conductive additives, and fabrication of composite electrodes.

Manuscript submitted December 19, 2016; revised manuscript received January 20, 2017. Published February 4, 2017. *This paper is part of the JSS Focus Issue on Nanocarbons – In Memory of Sir Harry Kroto.*

Electrochemical capacitors are widely studied due to their affordable and efficient electrical energy storage which is needed to enable widespread use of renewable energy sources and provide energy security.[1] These devices strive to solve energy issues by providing quick charge-discharge (millisecond to second time constants), high power densities and long cycle lives. Mainly due to the mechanism by which charge is stored, these devices, unlike batteries, store energy by physical adsorption of ions leading to the formation of the electric double layer on the electrode. Due to the performance metrics necessary to achieve functioning devices, the electrode is commonly made from highly conductive, thermally and electrically stable, large surface area carbon materials such as activated carbon (AC), and carbide-derived carbon (CDC).[1] Carbon black or carbon nanotubes are often added to the activated carbon and other electrode materials to improve their electronic conductivity and performance at high rates.[2] Another carbon material, onion-like carbon (OLC) has also shown promise in electrochemical capacitors because of a unique, multishell fullerene structure with nanoscale diameters (5–10 nm).[3–8] OLC can be considered as the ultimate carbon black because of its small particle size and high electrical conductivity. These materials have accessible and non-functionalized external surface areas, enabling the quick charging and discharging necessary for electrochemical capacitors.[3] Previously investigated OLC-based microsupercapacitors, fabricated with interdigitated architectures, achieved high-rate performance, delivered stack capacitances four orders of magnitude higher than that of electrolytic capacitors, and provided higher specific power compared to activated carbon.[5,9]

Recently, there has been increased interest in developing new and more efficient electrode fabrication methods for microsupercapacitors for applications such as on-chip power sources, wearable electronics, and many others.[10] One future method of microsupercapacitor fabrication could be realized through printing of carbon-based functional inks, preferably from commercial inkjet printers that can allow the process to be scaled up for printing many devices in a short time. However, inks must have specific properties to allow for the carbon to be successfully printed into a functioning device. One of the most important characteristics for successful ink formulation is the stability of the conductive active material in solution (the active material vehicle) and these stability parameters vary between printing technologies and printers.[11–13] Material properties of the conductive ink such as particle size, surface charge, and surface functionalization are all important characteristics that develop a fruitful functional ink. The carbon material must also be very conductive and provide decent rate performance since microsupercapacitors are often designed for high power applications. In this paper, we have chosen onion-like carbon (OLC), a carbon material derived from nanodiamond, which can operate up to 10 V/s and has a conductivity of $\sim$ 4 S/cm.[4] While single OLC particles are less than 10 nm in size, after synthesis from nanodiamond, they exist in larger agglomerates with sizes >500 nm. Also, being graphitic and hydrophobic, they tend to further aggregate in aqueous solutions. Previously, there has been effort focused on creating smaller OLC agglomerates that are stable and colloidal in aqueous media. Attrition milling of onion like carbon was reported using a wet dispersion in polyacrylic acid (PAA).[14] The resulting particles were smaller in size and were stabilized by the PAA that was in solution, allowing the particles to stabilize. Additionally, previous studies done on poorly soluble organic materials[15] and nanodiamond[16,17] showed a decrease in agglomerate sizes by salt-assisted attrition or ultrasonic milling. To qualify as a good media for milling, it has been shown that the size of the particles used for milling must be comparable in size to the particles being milled. In most reported cases, sodium chloride salt (NaCl) acts as an appropriate milling media for other materials and it can be easily removed from the mixture by washing with deionized water, an advantageous property which makes this process inexpensive and scalable. Moreover, previous work performed on other carbon nanomaterials, such as multi-walled carbon nanotubes (MWCNTs) showed that acid-oxidation assisted the nanomaterials to be dispersed in aqueous media. Through analysis by Raman spectroscopy, it was found that a mixture of nitric acid (HNO_3) and sulfuric acid (H_2SO_4) allowed for maximum Raman intensity of the G band of graphitic carbon.[18] The authors used a (1:1) HNO_3/H_2SO_4 acid ratio to acid-oxidize the MWCNTs at 110 degrees C for 24 hours.[18] Following this study was a systematic investigation of different oxidative treatments of MWCNTs, which concluded that a treatment in (1:3) mixture of HNO_3/H_2SO_4 conducted for 8 hours at 70°C produced the highest extent of oxidation (10.2 at.% of oxygen).[19] Following these techniques, creating a functional aqueous ink containing onion-like carbon is feasible.

To process the OLC to be more ideal for creating an ink, we used salt-assisted milling to break up the OLC agglomerates, similar to

*Electrochemical Society Fellow.
zE-mail: gogotsi@drexel.edu

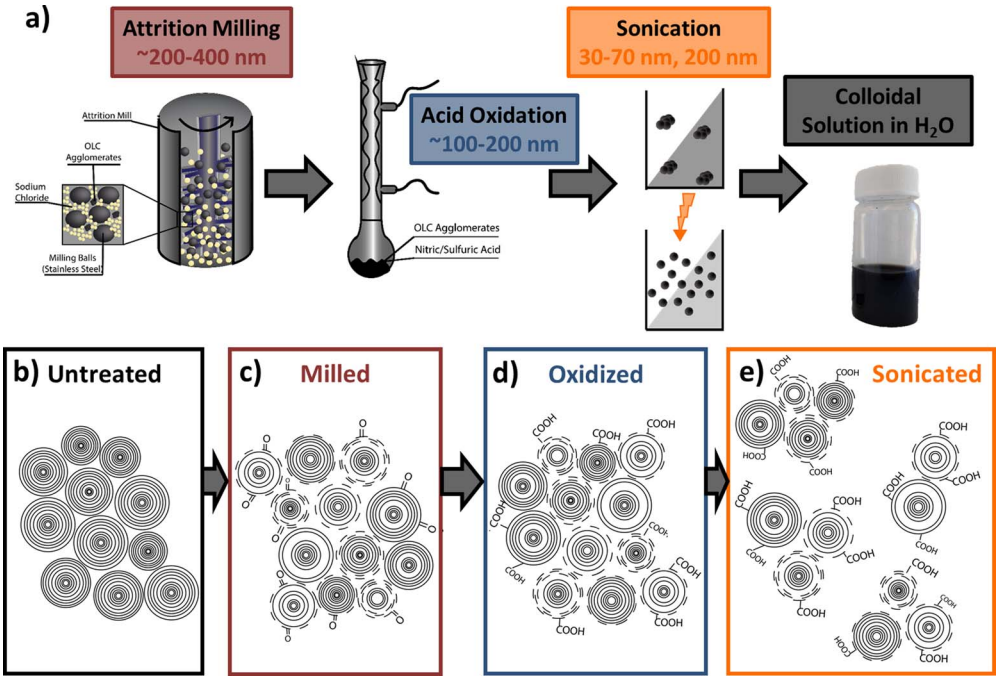

Figure 1. (a) Schematic showing the processing steps from raw OLC to the stable aqueous dispersion. Schematics of the OLC particles at the (b) untreated, (c) milled, (d) acid oxidized, and (e) sonicated stages.

previous studies on nanodiamond,[17] followed by acid oxidation to functionalize the surface with carboxyl groups that make the OLC dispersible in water. Finally, probe sonication was used to obtain an even smaller agglomerate size, around 100 nm. Together, these four processing steps were used to create a stable water-based ink of OLC particles from freshly synthesized OLC with large agglomerate sizes. As the ultimate idea was to use this ink to fabricate microsupercapacitors, the OLC product from each stage was measured in an electrochemical capacitor to test the effect of the processing steps on the performance. Overall, the capacitive performance of OLC was enhanced through the processing steps, in addition to the particle size decreasing, showing that effective inks can be formulated through materials processing.

Experimental

OLC synthesis.—OLC powders were synthesized from commercial nanodiamond precursor (UD90 grade, SP3 Diamond Technologies, USA) by annealing it in 10^{-6} torr vacuum at 1800°C for 3 hours.

OLC processing steps.—A complete schematic of the processing procedure is shown in Figure 1a, with schematics of the powder at each stage shown in Figs. 1b–1e. First, OLC powders were mixed in a 1:7 OLC to salt ratio and combined with 500 g of stainless steel balls (AISI 440-C, 1/4 inch or 0.635 cm diameter), similar to studies previously conducted on nanodiamond.[16] Using sodium chloride salt (NaCl) as the milling media, a temperature controlled attrition mill (Union Process Model HD01) was used to mechanically grind the OLC agglomerates and NaCl crystals. The milling was conducted for 5 hours at a speed of 41.5 Hz (500 RPM) at a constant temperature between 0 and −5°C. The temperature was kept cool to avoid heat exposure which could cause thermal damage. After milling, the OLC agglomerates were washed by deionized water to remove excess NaCl. A silver nitrate (0.1N) test was used to confirm the removal of salt by isolation of a small sample for testing. The remaining OLC agglomerates were filtered through a hydrophilic polypropylene membrane (Celgard) with 64 nm pore size to remove excess water, where the filtrate liquid was clear. The powder was then dried in a vacuum oven for ∼12 hours at 70°C. Oxidation of the OLC agglomerates was performed in a round-bottomed reflux condenser with a 200 mg OLC/10 mL acid with a 1:3 volume ratio of nitric acid (HNO_3) and sulfuric acid (H_2SO_4). A condenser tube was fastened on the top, and the reaction started when the first reflux drop was observed. In this reaction, a color change is observed shortly after beginning due to the reaction between OLC carbon particles, nitric, and sulfuric acids. After exposure to acid for 5 hours at 70°C, the resulting solution was allowed to cool. The solution was then washed by vacuum filtering the dark solution over a 0.22 μm polyvinylidene fluoride (PVDF) filter (Durapore Membrane Filters) until the filtered solution reached neutral pH ∼6-7. During the first wash, the filtrate was translucent red-brown. Consecutive washing thereafter revealed mildly colored or clear solutions. It is best to note that smaller agglomerates of OLC may have passed through the filter membrane, leading to loss of product and an average particle size that is higher than the true processing capability. After washing of acid, the OLC powder was dried in a vacuum oven at 70°C for approximately 12 hours. The dried powder was redispersed in deionized water. Bath and probe sonication methods were utilized to further decrease the agglomerate size of OLC. A solution containing OLC and water was bath sonicated (40 kHz frequency) for 30 minutes to begin the redispersion process and break up the largest agglomerates of OLC that occur during acid oxidation. The solution was then probe sonicated for 1 hour to further decrease the size of agglomerates. Finally, the solution was centrifuged for 15 minutes at 3500 RPM to allow the largest agglomerates to fall to the bottom, isolating the smallest particles in the solution supernatant. Yield in this process was variable, but in most cases after treating 200 mg in acid-oxidation, 75–80% OLC mass was retained.

OLC characterization.—Each processing step (milling, acid-oxidation, and sonication) was characterized by Scanning Electron Microscopy (SEM, Zeiss Supra 50VP) and Energy Dispersive Spectroscopy (EDS, Oxford) to evaluate powder morphology and composition, respectively. Fourier Transform Infrared Spectroscopy (FTIR) was performed on powder samples (Perkin-Elmer Spectrum One FTIR with attenuated total reflectance (ATR) accessory). Particle size analysis, zeta potential and electrophoretic mobility measurements were conducted using a Malvern Zetasizer Nano ZS (Malvern Instruments, USA). The powders were taken from the vacuum oven and redispersed

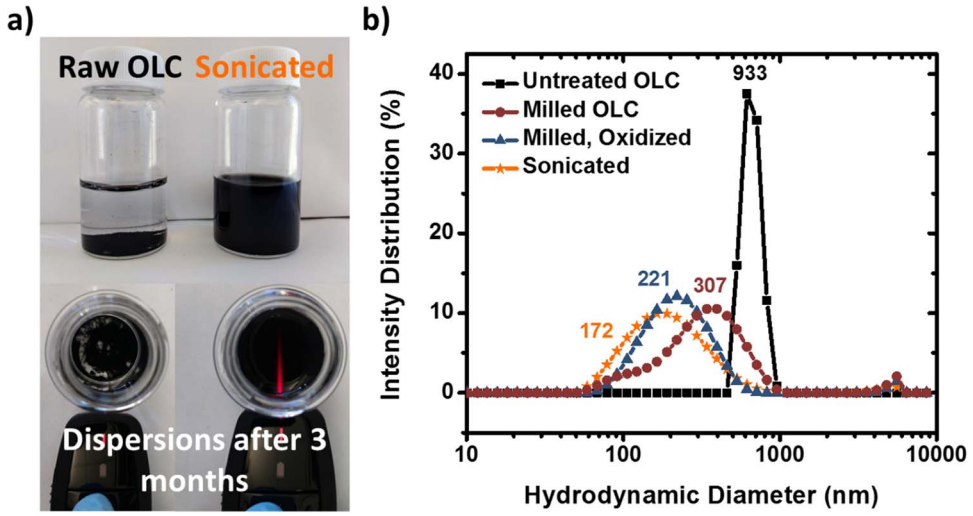

Figure 2. (a) OLC dispersions after 3 months for raw OLC powder in water (left) and OLC powder after all stages (right). The Tyndall effect is apparent for treated dispersions (bottom). (b) The intensity particle size distribution of the dispersions at all stages of processing, where the Z-average is labeled for each curve.

in deionized water at a 0.1 mg/mL concentration for particle size and zeta (ζ) potential analysis. The colloidal solutions were mildly sonicated for 10 minutes to allow the particles to redisperse before analysis. The particle size of each step (raw, milled, acid-oxidized, and post-processed) was measured using the same conditions (averaged over three measurements). For zeta potential and electrophoretic mobility, a plastic, disposable zeta-potential cell was used for each measurement (DTS1060, Malvern Instruments) and the measurements were averaged over three separate runs. The surface area and pore size of OLC were analyzed by isothermal nitrogen gas adsorption using liquid nitrogen as the coolant. Specific surface areas (SSA) for the products of each processing step were calculated by fitting the N_2 adsorption-desorption data using Brunauer-Emmett-Teller (BET) theory. Pore size distributions for each sample were determined by Quenched Solid Density Functional Theory (QSDFT) slit pore fitting of the gas sorption data. Raman spectroscopy was performed on a Renishaw inVia (UK) microspectrometer equipped with a 632.8 nm He-Ne laser with ~ 1 mW power, 63× magnifying objective with 0.7 numerical aperture, and a 1200 lines/mm grating.

Electrochemical characterization.—OLC electrodes were prepared with an addition of 5 wt% polytetrafluoroethylene (PTFE) binder and the resulting OLC/PTFE composite was mechanically rolled to a thickness of ~100 μm. Film electrodes were tested in a three-electrode Swagelok cell (Fig. S1). OLC electrodes, with platinum disks as current collectors, were used as the working electrodes and overcapacitive activated carbon electrodes, also using platinum disks as current collectors, were used as counter electrodes. A silver/silver chloride wire (Ag/AgCl) in 3.5 M potassium chloride (KCl) was used as the reference electrode. The working and counter electrodes were separated by a hydrophilic, surfactant-treated polypropylene Celgard membrane (Celgard 3501, Celgard) that was ~ 50 μm in thickness. All electrochemical tests were performed in 6 M potassium hydroxide (KOH) electrolyte. The capacitive performance of the OLC products from each processing step was evaluated using cyclic voltammetry and electrochemical impedance spectroscopy (EIS) using a BioLogic VMP3 potentiostat (BioLogic, USA). Cyclic voltammetry was performed at scan rates from 5 mV/s to 10 V/s and the capacitance of the OLC electrodes was calculated by integration of the discharge current (when current vs. time is below zero) with respect to time:

$$C\left(F/g\right) = \left(\int_0^t i\,dt\right) / (V * m),$$

where C is the specific capacitance (normalized to the mass of the working electrode), t is the discharge time, i is the discharge current, V is the voltage window, and m is the mass of the working electrode. All cyclic voltammograms (CVs) shown have been normalized by dividing the current of the original i-V curves by the applied scanning rate and working electrode mass. The positive and negative capacitance in the resulting CVs represent the charge and discharge capacitance, respectively. Electrochemical impedance spectroscopy was performed in the same three-electrode setup at frequencies from 10 mHz to 200 kHz with a sinusoidal potential amplitude of 10 mV around open circuit voltage.

Results and Discussion

Dispersibility and functionalization.—As depicted in Figure 2a, raw OLC does not effectively disperse in water, as the particles readily sediment, attributed to the bare (unfunctionalized), hydrophobic OLC agglomerates. However, processed OLC (milled, acid-oxidized, and sonicated) does exhibit stability in aqueous media, proven by the Tyndall effect. This effect shows the formation of a colloidal solution that can be accredited to a few material properties such as particle size, zeta potential, and surface functionalization. After milling, the particle size intensity distribution shows a reduction in particle size (Fig. 2b), from raw OLC exhibiting an average agglomerate size of 933 nm to milled samples showing an average size of 308 nm. The reduction in size continues through processing, as sonicating OLC agglomerates further reduces the average to 172 nm. It is worth noting that these particles are still OLC agglomerates (individual OLC particles are <10 nm in size) and sonication could be continued, hypothesized to decrease the agglomerate sizes further, while also inducing disorder. Furthermore, acid-oxidation offers two advantages: 1) removal of contaminants, and 2) surface functionalization or activation. When subjecting the acid-oxidized particles to a magnet, the impurities no longer responded, indicating the removal of magnetic particles, such as iron, which were introduced during the milling step. As proven by EDS, iron contaminants were completely removed via the HNO_3/H_2SO_4 etching (Table I). Additionally, to disperse in water, the particles must become hydrophilic, thus more polar. Polarity increases with the addition of oxygen-containing (e.g., carbonyl) functional groups. As noted by EDS, oxygen-containing functionalities are introduced during milling, and preserved, with carboxyl groups added during acid-oxidation and sonication. The resulting solution contains ~10 at.% oxygen (negatively charged surface groups). Furthermore, FTIR (Fig. S2) shows a relatively bare surface chemistry for untreated OLC. After milling and acid oxidation, changes in spectra reveal a

Table I. Energy dispersive X-ray spectroscopy results for OLC after each processing step.

Element	Untreated OLC (at.%)	Milled OLC (at.%)	Acid-Oxidized (at.%)	Sonicated (at.%)
C	95.7	86.9	90.4	89.2
O	4.2	11.1	9.6	10.7
Fe	0.1	2.0	0.0	0.1
Total	100	100	100	100

weak carbonyl peak ~1700 cm^{-1}, indicative of the introduction of polar surface functionalities which aide colloidal stability in aqueous media.

Electrophoretic mobility and zeta potential measurements can often act as a way to measure the extent of surface functionalization, due to functional groups often leading to particle surface charges.[20] After short exposure to milling and acid treatment, the absolute electrophoretic mobility increases (abs |x|), due to the presence of functional groups, such as negatively charged, oxygen-containing functional groups (Fig. S3). Prior to milling, the absolute value of the electrophoretic mobility is ~0.5 μmcm/Vs with a ζ-potential equal to −6.43 mV, suggesting poor colloidal stability (Fig. 2). After milling, the mobility increases to 3.56 μmcm/Vs and the ζ-potential stabilizes at −45.4 mV, signifying good colloidal stability (Fig. 2b). After further treatment, the electrophoretic mobility and ζ-potential continue to increase, confirming that the solution obtains colloidal stability due to the processing modifications. As particles in solution are dependent on the balance of charges (attractive vs. repulsive), information about agglomeration, sedimentation, etc. can be gathered from ζ-potential measurements. Sedimentation of raw OLC occurs due to the ζ-potential being close to zero. In this case, the particles have little to no surface charge, giving them no reason to stay stabilized in the water, which contains partially positive (δ+) and partially negative (δ−) disassociations. In the case of the treated sample, the negatively charged particles are mutually repelling each other, thus staying dispersed in water, however, if particles were attracted to one another, they would eventually gain enough mass to fall out of solution as sedimentation. Sedimentation does occur for raw OLC, however after processing conditions, such as acid oxidation and sonication, long term stability (>4 months) in aqueous media was achieved (Fig. 2a).

Electrochemistry.—Since the final application of dispersed carbon inks is potential electrochemical energy storage devices, the OLC was tested in a supercapacitor device at each stage of processing. Figures 3a–3c show the electrochemical results from these tests, including cyclic voltammograms, normalized by mass, cycled at 10, 200, and 1000 mV/s. From the CV curves, the increase in performance is especially evident after milling, specifically at the lower scan rates. Acid-oxidation and sonication further improve the shape of the CV

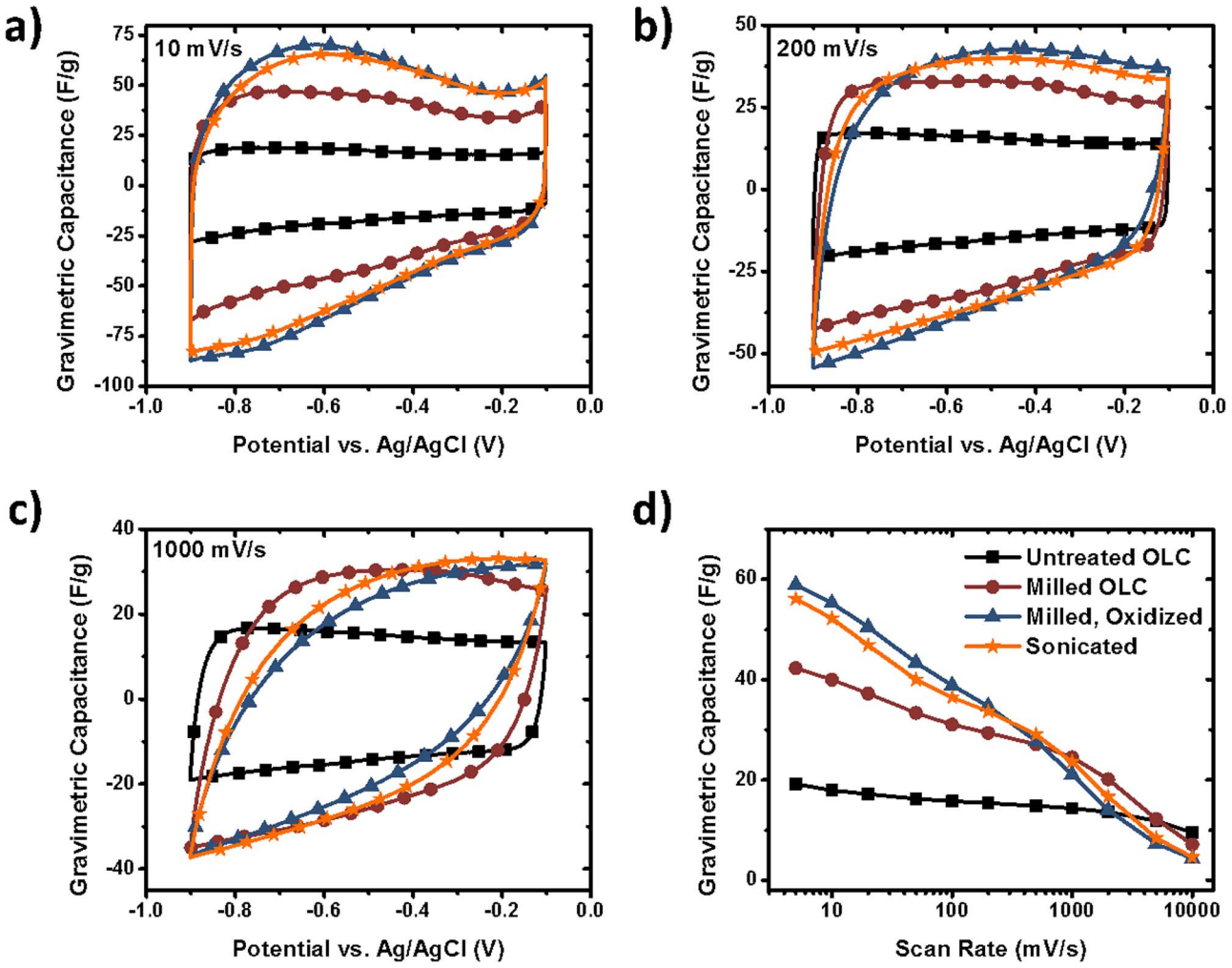

Figure 3. Electrochemical performance of the OLC at different stages, tested in a three-electrode cell with 6 M KOH. Cyclic voltammograms are shown for all four stages at (a) 10 mV/s, (b) 200 mV/s, and (c) 1000 mV/s scan rates. (d) Capacitive performance as a function of scan rate for the supercapacitors made from the OLC at all four stages.

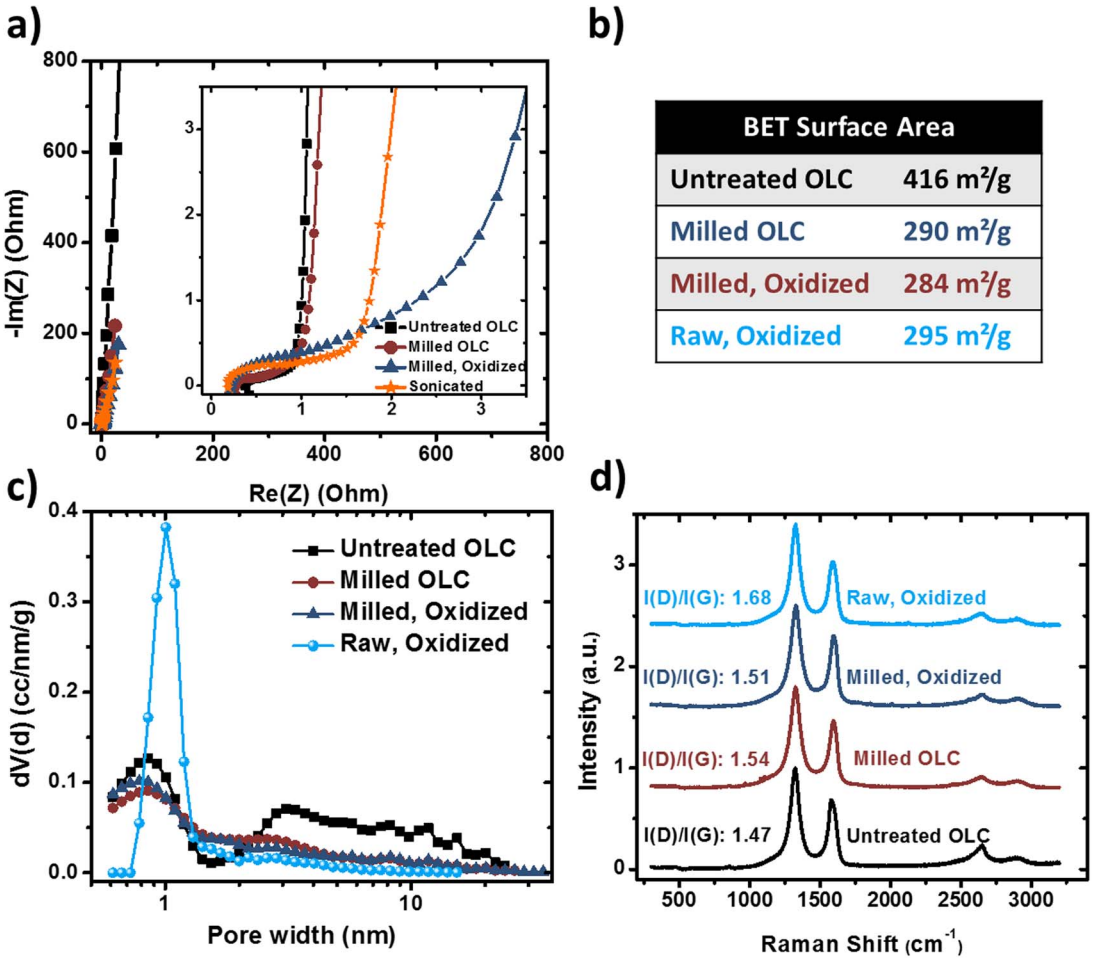

Figure 4. (a) Nyquist plot of three-electrode cells made with OLC after each processing step. (b) Specific surface area for OLC at different stages calculated using the BET theory. (c) Pore size distributions of OLC at each stage calculated from QSDFT. (d) Raman Spectroscopy of the OLC material at different stages with I(D)/I(G) ratios indicated.

curves, retaining the increase in capacitance that was achieved after milling. Figure 3d summarizes the capacitive performance of the four materials at different scan rates, pushing it to even 10 V/s. Known as a high rate performing material, untreated OLC performs consistently over the whole range of scan rates. Due to the outer surface structure of the OLC particles, ion adsorption can occur very quickly without diffusion limitations in a porous network. On the other hand, the final processed material has a capacitance that is almost three times higher than the untreated OLC at low scan rates. Specifically, at 10 mV/s the gravimetric capacitance is 19 F/g for untreated OLC and 52 F/g after the final sonication step. Each processing step performed serves to reduce the size of OLC agglomerates for improving the stability of OLC solutions, but during this process the number of inter-particle contacts also decreases. This effect paired with the increased structural disorder and oxygen content of the acid treated samples will have negative effects on capacitance retention at higher scan rates. This large disparity disappears at very high scan rates (>2 V/s) and the benefits gained by having a stable, aqueous OLC suspension outweigh the small loss in capacitance at very high scan rates. Figure 4a shows Nyquist plots for each of the OLC materials tested electrochemically. Each material shows similar behavior at high and low frequencies, with the plots for each material showing small real axis intercepts at high frequencies and close to vertical lines in low the frequency regions, which is indicative of close to ideal capacitive behavior. The major differences seen in the Nyquist plots occur in the mid-frequency region, where the mid-frequency capacitive behavior is right shifted on the real axis for the acid-oxidized and sonicated samples. This behavior can potentially be explained by the high amount of oxygen containing groups, especially carboxyl groups introduced to the OLC during chemical activation that can impede access of the electrolyte to the electrode surface. This is not seen in the milled sample, which has a similar oxygen content to the acid treated samples (Table I), which can partially come from iron oxides. To confirm that the increase in performance was not only due to the introduction of oxygen during acid treatment, we acid-oxidized the raw OLC without the milling step in between. The compared performance of these materials is shown in Figure S4a, where CVs are shown for 10 and 200 mV/s for untreated and oxidized OLC (Fig. S4a). In this case, the oxidized OLC retains the same CV shape characteristic of double-layer capacitors and maintains the rectangular profile, which suggests a low material resistance which is also a property of OLC. Defects introduced by milling and oxidation in acid, as well as surface coverage by -COOH, produce pseudocapacitive contribution that is clearly seen at low rates (Fig. 3a). This performance over different rates is shown in Figure S4b, where the oxidized OLC has a slightly lower capacitance but has the same fade profile across increasing rates as the untreated OLC.

Surface area and pore size distribution.—Typically, OLC can reach surface areas of 600 m^2/g with complete conversion from precursor nanodiamond.[4] Some processing techniques, such as chemical activation of the surface, can reach surface areas of 800 m^2/g, with defective outer-shell OLCs.[21] However, in this case, BET surface area decreases with processing (Fig. 4b), which may be in fact due to the presence of oxygen on the OLC, which blocks the gas from adsorbing

onto the surface, leading to a lower value. Initially after milling, the OLC material shows a surface area of 290 m^2/g (originally 416 m^2/g) and maintains this value even after acid-oxidation. Comparing pore size distributions of these three processing steps (Fig. 4c), we can identify that raw OLC had the largest distribution of pore sizes, with a large portion of pores being mesopores (>2 nm). After milling and oxidation, the volume of mesopores decreases relative to the intensity of the sub-nanometer pores (Fig. 4d). This can possibly be again explained by blocking of the pores due to iron oxide contamination or oxygen functional groups, lowering the measured BET surface areas. In addition, the surface area and pore size distribution were measured for the raw, oxidized sample to see what impact only the oxidation process has on the surface characterization. Results showed that in this case, the acid-oxidation decreased the BET surface area to 295 m^2/g, comparable to results of acid-oxidized and milled samples. Finally, to confirm that after all the processing steps, we still had the same level of graphitization, we used Raman spectroscopy to look at the I(D)/I(G) ratios at different stages (Fig. 4d). According to the Raman spectra, the G peak shifts slightly from 1587 cm^{-1} (untreated OLC) to 1594 cm^{-1} (milled, oxidized). This shift suggests the presence of defects from milling and oxidation. However, as the I(D)/I(G) ratio only increases from 1.47 to 1.51, the OLC is still highly graphitized and has not become fully amorphous carbon throughout the processing steps. This is also supported by the fact that the 2nd order Raman peaks, which are not present in disordered carbons, remained intact after milling and further processing (Fig. 4d).

Conclusions

The dispersion stability and electrochemical activity has been evaluated on milled, acid-oxidized, and sonicated onion like carbon. The resulting solution contains OLC agglomerates, which are of decreased size, increased surface functionalization and stabilization in aqueous media compared to the as-produced state. Processing OLC can allow for the development of OLC in aqueous applications, as an ink for functional devices, a coating, or as a component of a composite.

Acknowledgments

The authors acknowledge Taron Makaryan for assistance with Raman spectroscopy. This work was funded by the Fluid Interface Reactions, Structures and Transport (FIRST) Center, an Energy Frontier Research Center funded by the U.S. Department of Energy, Office of Science, Office of Basic Energy Sciences.

References

1. P. Simon and Y. Gogotsi, Materials for electrochemical capacitors. *Nat Mater*, **7**(11), 845 (2008).
2. Y. Gogotsi, Not just graphene: The wonderful world of carbon and related nanomaterials. *MRS Bulletin*, **40**(12), 1110 (2015).
3. J. K. McDonough and Y. Gogotsi, Carbon Onions: Synthesis and Electrochemical Applications. *Electrochem. Soc. Interface*, **22**(3), 61 (2013).
4. M. Zeiger, N. Jackel, V. N. Mochalin, and V. Presser, Review: carbon onions for electrochemical energy storage. *Journal of Materials Chemistry A*, **4**(9), 3172 (2016).
5. D. Pech, M. Brunet, H. Durou, P. Huang, V. Mochalin, Y. Gogotsi, P. L. Taberna, and P. Simon, Ultrahigh-power micrometre-sized supercapacitors based on onion-like carbon. *Nat Nanotechnol*, **5**(9), 651 (2010).
6. M. E. Plonska-Brzezinska and L. Echegoyen, Carbon nano-onions for supercapacitor electrodes: recent developments and applications. *Journal of Materials Chemistry A*, **1**(44), 13703 (2013).
7. Y. V. Butenko, L. Siller, and M. R. C. Hunt, Carbon onions. In *Carbon Nanomaterials*, 406 2 ed.; Y. Gogotsi; V. Presser, Eds. CRC Press: pp. 1–18, 2013.
8. D. M. Anjos, J. K. McDonough, E. Perre, G. M. Brown, S. H. Overbury, Y. Gogotsi, and V. Presser, Pseudocapacitance and performance stability of quinone-coated carbon onions. *Nano Energy* **2**(5), 702 (2013).
9. J. K. McDonough, A. I. Frolov, V. Presser, J. J. Niu, C. H. Miller, T. Ubieto, M. V. Fedorov, and Y. Gogotsi, Influence of the structure of carbon onions on their electrochemical performance in supercapacitor electrodes. *Carbon*, **50**(9), 3298 (2012).
10. M. Beidaghi and Y. Gogotsi, Capacitive energy storage in micro-scale devices: recent advances in design and fabrication of micro-supercapacitors. *Energy & Environmental Science*, **7**(3), 867 (2014).
11. F. Bonaccorso, A. Bartolotta, J. N. Coleman, and C. Backes, 2D-Crystal-Based Functional Inks. *Adv Mater*, **28**(29), 6136 (2016).
12. S. D. Hoath, *Fundamentals of Inkjet Printing: The Science of Inkjet and Droplets*. Wiley-VCH: Delaware, 2015; Vol. **1**.
13. G. Cummins and M. P. Y. Desmulliez, Inkjet printing of conductive materials: a review. *Circuit World*, **38**(4), 193 (2012).
14. J. Y. Lee, K. H. Cho, D. P. Lim, Y. B. Lee, and D. S. Lim, Effect of attrition milling on dispersion of onion like carbon in aqueous medium. *Appl Phys a-Mater*, **88**(4), 693 (2007).
15. V. N. Mochalin, A. Sagar, S. Gour, and Y. Gogotsi, Manufacturing nanosized fenofibrate by salt assisted milling. *Pharm Res*, **26**(6), 1365 (2009).
16. A. Pentecost, S. Gour, V. Mochalin, I. Knoke, and Y. Gogotsi, Deaggregation of nanodiamond powders using salt- and sugar-assisted milling. *ACS Appl Mater Interfaces*, **2**(11), 3289 (2010).
17. K. Turcheniuk, C. Trecazzi, C. Deeleepojananan, and V. N. Mochalin, Salt-Assisted Ultrasonic Deaggregation of Nanodiamond. *ACS Appl Mater Interfaces*, **8**(38), 25461 (2016).
18. S. Osswald, M. Havel, and Y. Gogotsi, Monitoring oxidation of multiwalled carbon nanotubes by Raman spectroscopy. *J Raman Spectrosc*, **38**(6), 728 (2007).
19. K. A. Wepasnick, B. A. Smith, K. E. Schrote, H. K. Wilson, S. R. Diegelmann, and D. H. Fairbrother, Surface and structural characterization of multi-walled carbon nanotubes following different oxidative treatments. *Carbon*, **49**(1), 24 (2011).
20. R. J. Hunter, *Zeta Potential in Colloid Science: Principles and Applications*. Academic Press: UK, 1988.
21. Y. Gao, Y. S. Zhou, M. Qian, X. N. He, J. Redepenning, P. Goodman, H. M. Li, L. Jiang, and Y. F. Lu, Chemical activation of carbon nano-onions for high-rate supercapacitor electrodes. *Carbon*, **51**, 52 (2013).